Journal of Clinical and Translational Hepatology **2026**
DOI: 10.14218/JCTH.2026.00072

Original Article

Targeting the 4EBP1/HSP90β/Nrf2 Axis Sensitizes β-catenin-mutant Hepatocellular Carcinoma to mTOR Inhibitors via Ferroptosis Induction

Rong Li[1#], Yi Zhou[2#], Zimu Wang[3], Gang Liu[3], Deyu Fan[3], Lanxuan Huang[4], Fule Deng[5], Ning Wei[6], Runze Shang[7*] and Meng Xu[5*]

[1]Department of Anesthesiology, The Second Affiliated Hospital of Xi'an Jiaotong University, Xi'an, Shaanxi, China; [2]Department of Infectious Diseases, the First Affiliated Hospital of Xi'an Jiaotong University, Xi'an, Shaanxi, China; [3]Xi'an Jiaotong University Health Science Center, Xi'an Jiaotong University, Xi'an, Shaanxi, China; [4]Department of Oncology, The Second Affiliated Hospital of Xi'an Jiaotong University, Xi'an, Shaanxi, China; [5]Department of General Surgery, The Second Affiliated Hospital of Xi'an Jiaotong University, Xi'an, Shaanxi, China; [6]College of Animal Science and Technology, Northwest A&F University, Xi'an, Shaanxi, China; [7]Department of General Surgery, Affiliated Strait Hospital of Huaqiao University, Huaqiao University, Quanzhou, Fujian, China

Received: January 27, 2026 | **Revised:** April 15, 2026 | **Revised:** May 21, 2026 | **Published online:** June 16, 2026

Abstract

Background and Aims: The aberrant activation of the mTOR pathway and its crosstalk with other signaling cascades represent key drivers of hepatocellular carcinoma (HCC) progression. mTOR-mediated ferroptosis suppression has been implicated in HCC resistance to chemotherapy. This study aimed to elucidate the mechanisms underlying mTOR inhibitor resistance and to evaluate the therapeutic potential of multidrug combinations in β-catenin-mutant HCC. ***Methods:*** MHCC97H and SNU449 cells were transfected with 4EBP1WT, 4EBP1A4, or HSP90β expression plasmids and then treated with rapamycin to assess their effects on ferroptosis and rapamycin sensitivity. The role of 4EBP1 in regulating ferroptosis was further explored by Western blotting, co-immunoprecipitation, and immunofluorescence. The inhibitory effects of mTOR inhibitors (rapamycin, MLN0128), ERK inhibitors (PD901), and their combination (MLN0128 + PD901) on tumor cells were evaluated. HCC mouse models were generated via hydrodynamic tail vein injection of c-Met/β-cateninΔN90 or c-Met/β-cateninΔN90/4EBP1A4 plasmids to evaluate the therapeutic effects of the four treatment regimens. ***Results:*** Rapamycin more potently inhibited mTOR/RPS6 than mTOR/4EBP1 and concurrently induced ferroptosis. 4EBP1A4 promoted ferroptosis and potentiated rapamycin efficacy. Mechanistically, 4EBP1A4 competitively bound HSP90β, displacing Keap1, thereby increasing Keap1–Nrf2 complex formation and promoting Nrf2 degradation. Furthermore, rapamycin, MLN0128, PD901, and their combination reduced p-4EBP1 levels, induced ferroptosis, and inhibited HCC cell proliferation, thereby suppressing tumor growth, with the combination exhibiting the strongest effect. ***Conclusions:*** 4EBP1A4 enhances Nrf2 ubiquitination and degradation via the HSP90β/Keap1 axis, relieving mTOR-mediated ferroptosis suppression and synergistically improving rapamycin efficacy. Additionally, rapamycin, MLN0128, and PD901 suppress HCC progression by inducing ferroptosis, with their combination showing superior potency.

Citation of this article: Li R, Zhou Y, Wang Z, Liu G, Fan D, Huang L, *et al*. Targeting the 4EBP1/HSP90β/Nrf2 Axis Sensitizes β-catenin-mutant Hepatocellular Carcinoma to mTOR Inhibitors via Ferroptosis Induction. J Clin Transl Hepatol 2026. doi: 10.14218/JCTH.2026.00072.

Introduction

Hepatocellular carcinoma (HCC), accounting for 85–90% of primary liver cancer cases, represents the most prevalent hepatic malignancy worldwide. HCC is characterized by an asymptomatic early stage and rapid progression, resulting in the majority of patients presenting with locally advanced disease at diagnosis and consequently missing the optimal window for surgical resection.[1] Contemporary HCC treatment paradigms, particularly first-line chemotherapy and rational combination strategies, have achieved unprecedented clinical outcomes, significantly improving objective response rates and disease control rates, as well as prolonging both progression-free survival and overall survival.[2,3] Nevertheless, drug resistance remains a major challenge in clinical treatment.[4] Moreover, high toxicity and adverse effects, coupled with the lack of reliable biomarkers, further limit the clinical application of combination therapies.[5] Therefore, it is imperative to investigate the molecular mechanisms of HCC chemotherapy, develop more precise biomarkers, and ex-

Keywords: Hepatocellular carcinoma; HCC; 4EBP1; mTOR pathway; Ferroptosis; Drug combination.

[#]Contributed equally to this work.

[*]**Correspondence to:** Meng Xu, Department of General Surgery, The Second Affiliated Hospital of Xi'an Jiaotong University, 157 Xiwu Road, Xi'an, Shaanxi 710004, China. Tel: +8602987679246, E-mail: miaoslnol041135@163.com; xm19912015@163.com; xu.meng@xjtu.edu.cn; Runze Shang, Department of General Surgery, Affiliated Strait Hospital of Huaqiao University, Huaqiao University, Quanzhou, Fujian 362021, China. ORCID: https://orcid.org/0000-0002-7958-0700. Tel: +86-18691093617, E-mail: runze.shang@hqu.edu.cn.

plore new treatment strategies.

Ferroptosis, a form of regulated cell death, depends on iron accumulation and lipid peroxidation. Notably, ferroptosis exhibits distinct advantages in overcoming drug resistance in HCC. For example, the combination of low-dose oxaliplatin and dihydroorotate dehydrogenase inhibitors effectively curbs HCC progression and alleviates chemotherapy toxicity by triggering ferroptosis.[6] Additionally, co-administration of fatty acid synthase inhibitors with sorafenib induces ferroptosis by suppressing the HIF1α/SLC7A11 pathway. This, in turn, reverses sorafenib resistance in HCC cells and enhances antitumor effects.[7] Nevertheless, given the intricate mechanisms and substantial heterogeneity inherent in HCC, developing more refined and accurate biomarkers remains imperative.

Tumor cell proliferation is closely associated with aberrant activation of the mTOR signaling pathway, which enhances protein translation efficiency and promotes metabolic reprogramming. Moreover, activation of the mTOR pathway suppresses ferroptosis, contributing to tumor cell drug resistance.[8] mTORC1 primarily phosphorylates S6K1, thereby activating RPS6 to facilitate protein synthesis and regulate cellular metabolic processes, ultimately promoting tumor cell proliferation. 4EBP1 is another key downstream effector of the mTOR signaling pathway. Upon phosphorylation by mTORC1, 4EBP1 dissociates from eIF4E, promoting assembly of the translation initiation complex and thereby modulating protein synthesis. In addition, 4EBP1 participates in the regulation of ferroptosis. By inhibiting mTOR and reducing 4EBP1 phosphorylation, sorafenib attenuates protein synthesis in HCC cells. Notably, 4EBP1 phosphorylation exhibits pathway promiscuity, with regulation by mTOR, AMPK, TGF-β, and ERK signaling.[9–11] Therefore, 4EBP1 represents a promising biomarker for combination therapy. Currently, preclinical studies demonstrate promising antitumor efficacy of mTOR inhibitor–based combination therapies across multiple malignancies. However, whether these combinatorial regimens can cooperatively trigger ferroptosis to overcome acquired resistance to mTOR inhibitors has yet to be systematically investigated.

Accordingly, this study explored 4EBP1-mediated ferroptosis regulation and evaluated its impact on rapamycin's therapeutic effects through both *in vitro* and *in vivo* experiments. Furthermore, we treated β-catenin-mutant HCC mice with mTOR inhibitors, MEK/ERK inhibitors, and their combination, and evaluated the effects of these regimens on ferroptosis and antitumor efficacy, to provide a theoretical basis for developing novel clinical treatment strategies for HCC.

Methods

Cell culture

MHCC97H and SNU449 cells were cultured in DMEM (Gibco, USA) supplemented with 10% fetal bovine serum, 100 U/mL penicillin, and 100 μg/mL streptomycin. Cultures were maintained in a humidified incubator at 37 °C with 5% CO_2.[12]

Cell transfection and treatment

4EBP1A4 is a non-phosphorylatable mutant in which T37, T46, S65, and T70 of 4EBP1 are mutated to alanine, while 4EBP1D4 is a constitutively phosphorylated mimetic mutant in which these sites are mutated to aspartic acid.[13] The pCMV-4EBP1WT, pCMV-4EBP1D4, and pCMV-4EBP1A4 plasmids were constructed and validated by Addgene (Watertown, MA). si-HSP90β was synthesized by GenePharma (Shanghai, China). The vector and pcDNA3.1-HSP90β plasmids were also constructed and verified by GenePharma. SNU449 and MHCC97H cells were seeded in 6-well plates at a density of 4×10^5 cells/well. Upon reaching approximately 60% confluence, pCMV-4EBP1WT (4EBP1WT), pCMV-4EBP1A4 (4EBP1A4), and pCMV-4EBP1A4 + pcDNA3.1-HSP90β (4EBP1A4 + HSP90β) were transfected into cells according to the Lipofectamine 2000 protocol (Thermo Fisher, USA). After 6 h, the medium was replaced with fresh culture medium, and the cells were cultured for an additional 48 h.[14] Furthermore, this study evaluated and compared the therapeutic efficacy of various pharmacological agents by treating HCC cells with rapamycin (25 μM, purity ≥ 98%, Yeasen Biotechnology, Shanghai, China), MLN0128 (5 μM, purity ≥ 98%, Yeasen Biotechnology), PD0325901 (PD901, 150 μM, purity ≥ 98%, Yeasen Biotechnology), and their combination (MLN0128 + PD901: 5 μM + 150 μM).[15]

Cell viability

SNU449 and MHCC97H cells were suspended in fresh medium at a density of 5×10^3 cells per well and seeded into 96-well plates. When confluence reached approximately 60%, plasmids were transfected into the cells. After 48 h of transfection, the cells were treated with rapamycin for 24 h. Subsequently, 10 μL of CCK-8 reagent (C0038, Beyotime, Beijing, China) was added to each well, and the plates were incubated in the dark at 37 °C with 5% CO_2 for 4 h. Finally, absorbance was measured at 450 nm using a microplate reader (Bio-Tek, USA). All experiments were performed in triplicate. Rapamycin was serially diluted to concentrations of 2 μM, 5 μM, 10 μM, 20 μM, 30 μM, and 60 μM. PD901 was applied at concentrations of 10 μM, 25 μM, 50 μM, 100 μM, 200 μM, and 300 μM under the same experimental conditions.[15]

Propidium iodide staining for detection of cell death

After cells were transfected and subsequently treated with rapamycin for 48 h, adherent cells were detached using trypsin without EDTA (Solarbio, Beijing, China). The cell pellet was collected and resuspended in pre-cooled 1× PBS. Subsequently, 1 mL of propidium iodide staining working solution (Thermo Fisher Scientific, USA) was added, and the mixture was incubated in the dark at room temperature for 30 min.[16] Finally, the cells were observed under a fluorescence microscope (Nikon Eclipse C1, Tokyo, Japan).

Detection of reactive oxygen species (ROS) levels

Total ROS and lipid ROS levels were detected using DCFH-DA (D6883, Sigma-Aldrich, USA) and BODIPY 581/591 C11 kits (Cat# S0043S, Beyotime, China), respectively.[17,18] After treatment, probe working solution was added at a final concentration of 5 μmol/L. The cells were incubated in the dark at 37 °C for 30 min, washed with PBS, and observed under a fluorescence microscope. Fluorescence intensity was analyzed using ImageJ software.

Western blotting

Western blot analysis was performed as previously described.[19] Briefly, cells were lysed using RIPA buffer, and protein concentration was quantified using a BCA assay kit (Beyotime Biotechnology, Shanghai, China). Protein samples were separated by SDS-PAGE and transferred onto PVDF membranes (Sevior Biotechnology, Wuhan, China) via electroblotting. Membranes were blocked with 5% non-fat milk at room temperature for 2 h, washed three times with TBST, and incubated overnight at 4 °C with primary antibodies (Table 1). They were then incubated with horseradish peroxidase-conjugated secondary antibodies for 2 h at

Table 1. Antibody Information

Antibody	Dilution ratio	Item number	Source
p-mTOR	1:500	ab109268	abcam (UK)
mTOR	1:1,000	ab32028	abcam (UK)
p-ERK	1:500	ab201015	abcam (UK)
ERK	1:1,000	ab184699	abcam (UK)
p-AKT	1:500	ab81283	abcam (UK)
AKT	1:1,000	ab8805	abcam (UK)
p-RPS6	1:1,000	#4858	Cell Signaling technology (USA)
RPS6	1:1,000	#2217	Cell Signaling technology (USA)
p-4EBP1(T37/46)	1:1,000	#2855	Cell Signaling technology (USA)
p-4EBP1(S65)	1:1,000	#9451	Cell Signaling technology (USA)
4EBP1	1:1,000	#9644	Cell Signaling technology (USA)
FTH1	1:1,000	ab287968	Abcam (UK)
GPX4	1:1,000	#59735	Cell Signaling technology (USA)
ACSL4	1:1,000	#38493	Cell Signaling technology (USA)
Ccnd1	1:1,000	ab134175	abcam (UK)
PCNA	1:1,000	ab92552	abcam (UK)
HSP90β	1:1,000	ab203085	abcam (UK)
Keap1	1:1,000	#8047	Cell Signaling technology (USA)
Nrf2	1:1,000	ab313825	abcam (UK)
GAPDH	1:1,000	ab181602	abcam (UK)

UK, United Kingdom; USA, United States of America

room temperature. Protein expression levels were detected using an enhanced chemiluminescence system (Amersham, UK) and quantified using Quantity One software (Bio-Rad, Hercules, CA, USA).

Co-immunoprecipitation (Co-IP) and ubiquitination

Cells were lysed in RIPA buffer, and 200 μL of lysate was reserved as the input sample. The supernatant was incubated with 2 μg anti-Flag antibody (MA5-27759, Thermo Fisher Scientific, USA) at 4 °C for 2 h. Subsequently, 25 μL protein G agarose beads (Thermo Fisher Scientific, USA) were added, and the mixture was incubated overnight at 4 °C.[20] The precipitate was then collected, resuspended in SDS-PAGE loading buffer, boiled for 10 min, and subjected to Western blot analysis.

The HA-tagged wild-type ubiquitin (HA-Ub-WT), ubiquitin containing only lysine 48 (HA-Ub-K48), and ubiquitin containing only lysine 63 (HA-Ub-K63) were cloned into the pCMV vector (constructed and validated by HeWu Biotechnology, Shanghai, China). Subsequently, Flag-Keap1 and Myc-Nrf2 plasmids were co-transfected with HA-Ub-WT, HA-Ub-K48, or HA-Ub-K63 into SNU449 and MHCC97H cells. Immunoprecipitation was performed using an anti-Flag antibody, and ubiquitination levels of immunoprecipitated proteins were detected using an anti-ubiquitin antibody (1:1,000, ab134953).[20]

Protein half-life assay

Cycloheximide (CHX, 100 μg/mL, Dingguo Changsheng, Beijing, China) was added to the culture medium after 48 h of siRNA transfection. The cells were then cultured in a 5% CO_2 incubator at 37 °C and collected at 0, 12, 24, 36, and 48 h after CHX treatment.[20] Nrf2 protein levels were detected by Western blotting.

Transmission electron microscopy

Transmission electron microscopy was performed as previously described.[21] Briefly, cells were collected and fixed with electron microscopy fixative at 4 °C (Solarbio, Beijing, China) for 4 h. Samples were then fixed with 1% osmium tetroxide (Solarbio, Beijing, China) for 2 h at room temperature and washed with PBS. Samples were dehydrated through a graded ethanol series (50%, 70%, 80%, 90%, 100%, and 100%) for 10 min each. After dehydration, samples were infiltrated with a mixture of acetone and 812 embedding resins (Solarbio, Beijing, China) for 24 h. The infiltrated samples were incubated overnight at 37 °C, followed by polymerization at 60 °C for 48 h. Ultrathin sections (60 nm) were prepared using an ultramicrotome and stained sequentially with 2% uranyl acetate in alcohol and lead citrate (Solarbio, Beijing, China) for 15 min each. After drying, sections were observed under a transmission electron microscope (JEM-1400Plus, JEOL, Tokyo, Japan).

Immunofluorescent staining

Cells were seeded at a density of 5×10^4 cells per well in confocal dishes placed in 6-well plates and cultured for 48 h. The immunofluorescent assay was performed as described previously.[21] Briefly, cells were fixed with 4% paraformaldehyde and permeabilized with 0.3% Triton X-100 (Beyotime, Shanghai, China). Subsequently, cells were incubated overnight at 4 °C with primary antibodies against Flag (1:1,000),

Myc (1:1,000), and Nrf2 (1:1,000). The following day, cells were incubated with fluorescence-labeled secondary antibodies at room temperature for 2 h. Nuclei were stained with DAPI (ab228549, Abcam). Finally, images were captured using an LSM880 confocal microscope (Leica, Germany).

GSH/GSSG assay

The GSH and GSSG Assay Kit (S0053, Beyotime, Beijing, China) was used according to the manufacturer's instructions.[22] Briefly, cells were mixed with protein removal reagent and subjected to three freeze–thaw cycles in liquid nitrogen. Total glutathione detection working solution and NADPH working solution (0.5 mg/mL) were added sequentially, and the mixture was incubated at 25 °C for 5 min. Absorbance was measured at 412 nm to determine total glutathione levels. Subsequently, GSH scavenging auxiliary solution and working solution were added, and the reaction was incubated at 25 °C for 60 min to determine GSSG content.

Iron assay

The concentration of ferrous iron (Fe^{2+}) was determined using a Ferrous Iron Colorimetric Assay Kit (Cat. No. E-BC-K139-M, Elabscience, Wuhan, China).[23] Briefly, 2×10^5 cells were seeded into 6-well plates. After 48 h, the supernatant was collected. Then, 75 μL of sample was mixed with 300 μL iron color reagent, and the mixture was centrifuged at 3,000 × g for 10 min at 4 °C. Absorbance was measured at 530 nm, and Fe^{2+} content was calculated based on a standard curve.

Mitochondrial membrane potential (ΔΨm) assay

Cells in the logarithmic growth phase were digested with trypsin and incubated with JC-1 working solution (M8650, Solarbio, Beijing, China) in the dark at 37 °C for 30 min. After three washes with pre-cooled JC-1 staining buffer, fluorescence intensity was quantitatively analyzed using ImageJ software.[18]

Animal experiments

pLenti-β-cateninΔN90 (N-terminal Myc-tagged), pLenti-c-Met, and pLenti-4EBP1A4 plasmids were used for the construction of the HCC model. Male wild-type FVB/N mice (6–8 weeks old) were purchased from Xi'an Jiaotong University and maintained in a specific pathogen-free facility with ad libitum access to food and water.

According to previous studies, the HCC mouse model was induced via hydrodynamic injection of c-Met and β-cateninΔN90 plasmids.[24,25] Briefly, plasmid mixtures (22.5 μg c-Met + 22.5 μg β-cateninΔN90, or 22.5 μg c-Met + 22.5 μg β-cateninΔN90 + 40 μg 4EBP1A4) were prepared in physiological saline and filtered through a 0.22 μm membrane. The solution was rapidly injected into the tail vein of FVB/N mice within 5–7 s. Five mice were euthanized at 4.7 weeks post-injection. Body weight and liver weight were recorded, and liver tissues were collected for analysis. The remaining mice were subjected to drug treatment. Rapamycin (6 mg/kg/day) or vehicle (a mixture of polyethylene glycol 400 and Tween 80) was administered by oral gavage for 6 days.[25] After 3 weeks of treatment, all mice were euthanized, and body and liver weights were measured, with liver tissues collected for histological and molecular analyses. In addition, vehicle, rapamycin (6 mg/kg/day), MLN0128 (0.5 mg/kg/day), MLN0128 (1 mg/kg/day), PD901 (10 mg/kg/day), and combination treatment (0.5 mg/kg MLN0128 + 10 mg/kg PD901) were administered by oral gavage. Treatment was initiated 4 weeks post-injection and continued for 3 consecutive weeks, and mice were sacrificed at 6.7 weeks post hydrodynamic injection.[15] A comprehensive evaluation and comparative analysis of therapeutic efficacy were subsequently performed. All animal protocols were approved by the Ethics Committee of Xi'an Jiaotong University (approval number: XJTUAE2025-1165).

Histology and immunohistochemistry

Tissue samples were fixed in 4% paraformaldehyde solution for 24 h. Tissues were subjected to routine dehydration, paraffin embedding, and sectioning (4–5 μm). Hematoxylin and eosin (H&E) staining was performed to evaluate the characteristics of neoplastic foci.[15] For immunohistochemistry, antigen retrieval was performed in a microwave oven using 10 mM citrate buffer (pH 6.0) at 100 °C for 20 min. Blocking serum was applied for 30 min to reduce nonspecific binding, and sections were incubated overnight at 4 °C with primary antibodies against Ki-67 (1:500), β-catenin (1:500), or Myc tag (1:500). After washing with PBS, sections were incubated with the corresponding secondary antibody for 2 h at room temperature. Signal was detected using the Vectastain ABC Elite kit (Vector Laboratories Inc.) and developed with DAB (Zhongshan Jinqiao, Beijing, China). Finally, sections were counterstained with hematoxylin, dehydrated, and mounted with neutral resin (Solarbio, Beijing, China).[20]

Statistical analysis

GraphPad Prism version 9.5.0 and SPSS Statistics 22.0 were used for data processing and statistical analysis. Data are presented as mean ± standard deviation. Student's t-test was used to assess differences between two groups. One-way or two-way analysis of variance was used to evaluate differences among multiple groups, followed by Tukey's post hoc test. $P < 0.05$ was considered statistically significant.

Results

Rapamycin induces ferroptosis and inhibits cell proliferation in HCC

MHCC97H and SNU449 cells exhibited markedly higher levels of p-mTOR and p-ERK than the normal hepatocyte line HL-7702 ($P < 0.0001$; Fig. 1A; Supplementary Fig. 1A). In MHCC97H and SNU449 cells, rapamycin treatment significantly reduced cell viability and induced cell death ($P < 0.05$; Fig. 1B and C; Supplementary Fig. 1B and C). Furthermore, the protein expression levels of p-mTOR, p-RPS6, p-4EBP1 (T37/46), and p-4EBP1 (Ser65) were significantly downregulated by rapamycin ($P < 0.05$), while p-ERK and p-AKT levels remained unchanged ($P > 0.05$; Fig. 1D; Supplementary Fig. 1D). Additionally, this study investigated the regulatory role of rapamycin in ferroptosis in SNU449 and MHCC97H cells. The results showed that protein levels of FTH1, GPX4, and SLC7A11 were significantly decreased, while ACSL4 levels were increased ($P < 0.05$; Fig. 1E; Supplementary Fig. 1E). Moreover, rapamycin significantly decreased the GSH/GSSG ratio, increased ROS levels, and promoted Fe^{2+} accumulation ($P < 0.05$; Fig. 1F–H; Supplementary Fig. 1F–H). Collectively, these results demonstrate that both the mTOR and ERK signaling pathways are concurrently activated in MHCC97H and SNU449 cells. Rapamycin effectively suppresses mTOR downstream signaling, preferentially inhibiting the mTOR/RPS6 axis over the mTOR/4EBP1 axis. Furthermore, rapamycin induces ferroptosis in tumor cells, thereby suppressing HCC cell proliferation.

Moreover, HCC mouse models were generated via hydrodynamic tail vein injection of c-Met/β-cateninΔN90, and rapamycin was used as a therapeutic intervention (Fig. 2A).

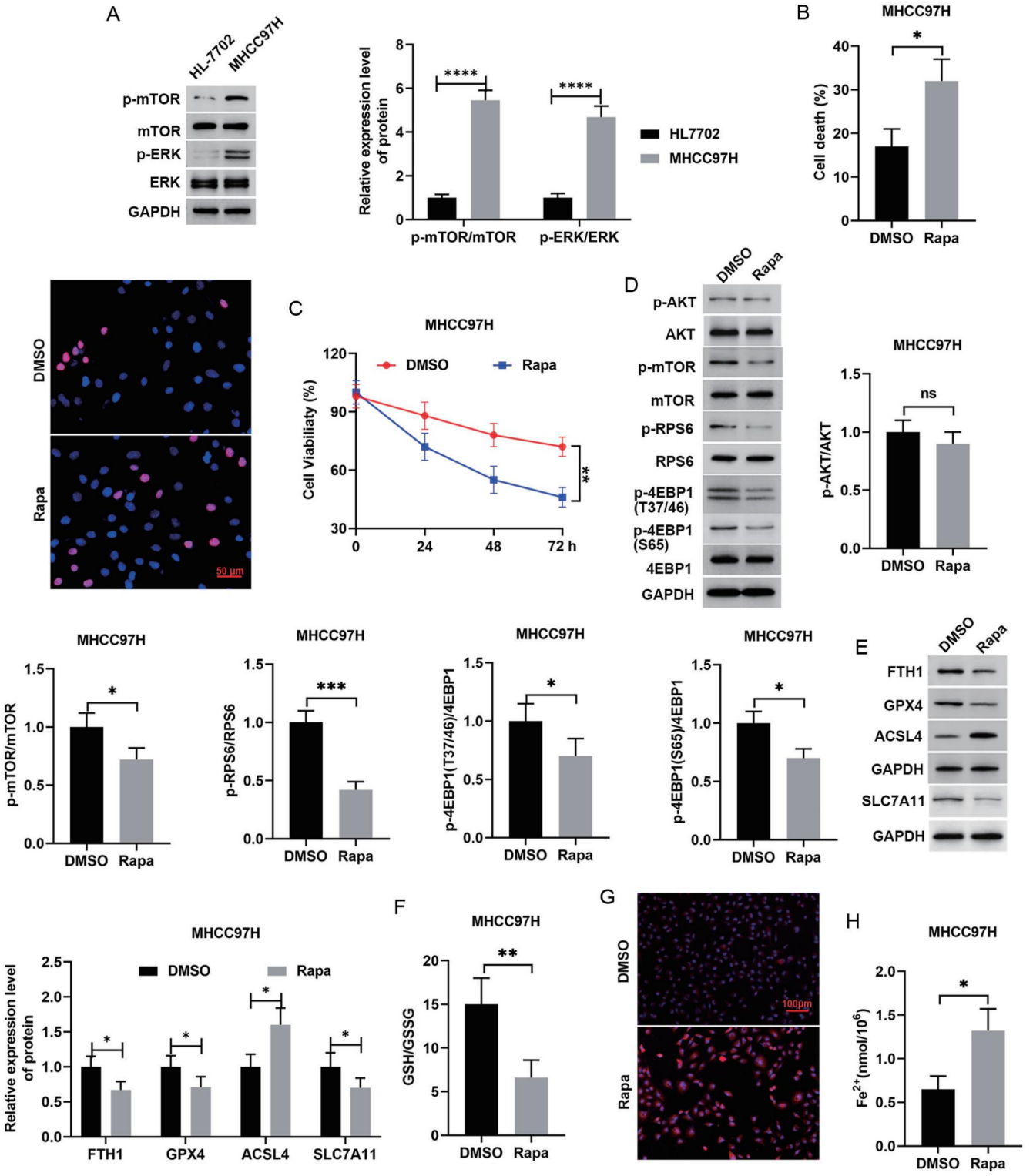

Fig. 1. Effects of rapamycin on ferroptosis and proliferation in HCC cells. (A) p-mTOR/mTOR and p-ERK/ERK proteins were assessed via Western blot assay. (B) Cell death was detected by PI staining (Scale bar: 50 μm). (C) Cell viability was assessed by CCK-8 assay. (D) mTOR pathway proteins were analyzed by Western blot assay. (E) Ferroptosis-associated protein levels were detected by Western blot assay. (F) The ratio of GSH/GSSG was detected using the GSH and GSSG Assay Kit. (G) Confocal microscopy detection of HCC cells stained with DCFH-DA (Scale bar: 100 μm). (H) Intracellular Fe^{2+} levels were measured using an iron assay kit. Each experiment was performed in triplicate. *P < 0.05, **P < 0.01, ***P < 0.001, and ****P < 0.0001. HCC, hepatocellular carcinoma; PI, propidium iodide; CCK-8, Cell Counting Kit-8; DCFH-DA, 2′,7′-dichlorofluorescein diacetate; DMSO, Dimethyl Sulfoxide; Rapa, rapamycin; GAPDH, glyceraldehyde-3-phosphate dehydrogenase.

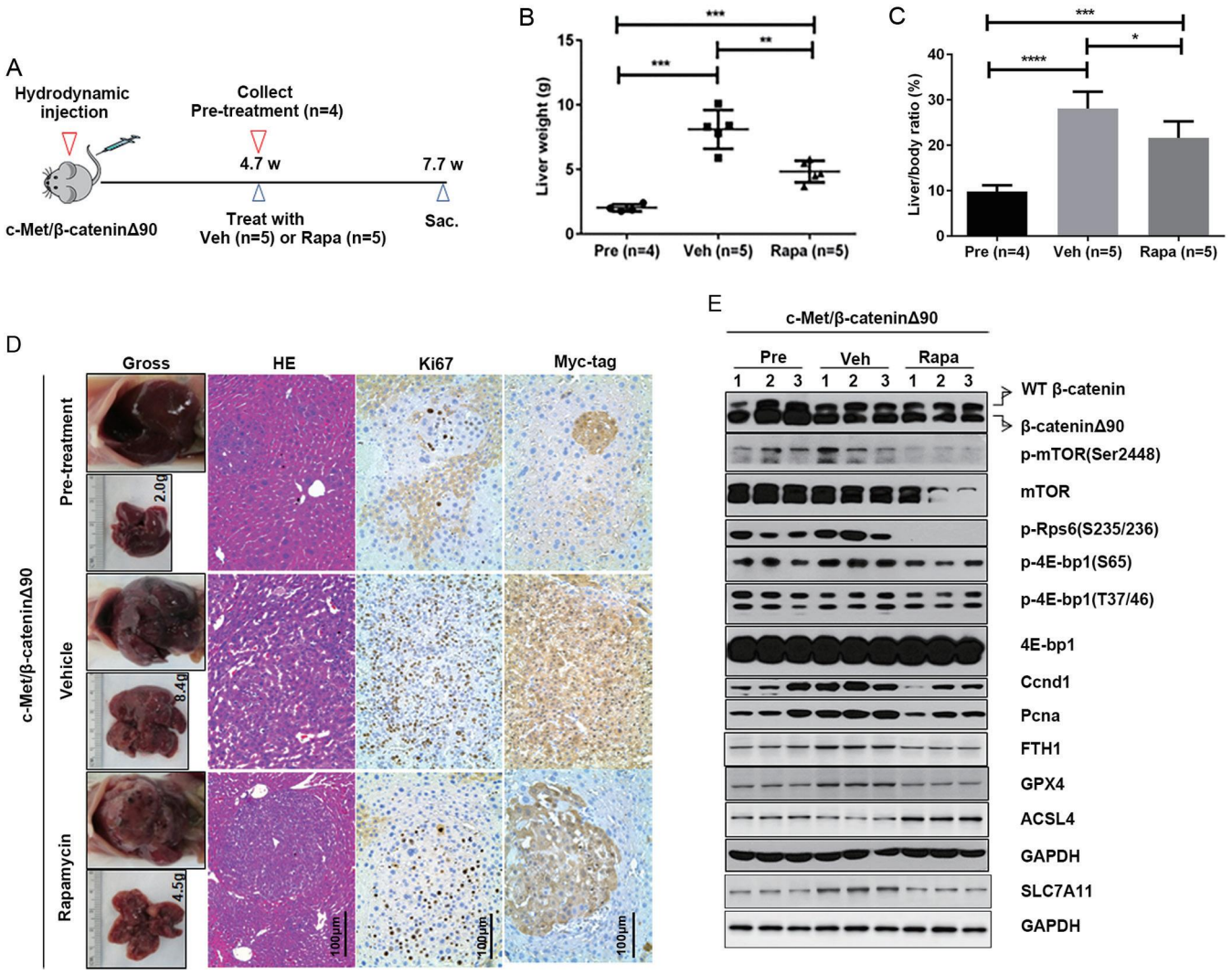

Fig. 2. Effects of rapamycin on tumor growth in HCC mouse models. (A) Study design. (B, C) Liver weight and liver/body ratio of c-Met/β-cateninΔ90-injected mice treated with Pre, Veh, and Rapa. (D) Gross, H&E images, β-cateninΔ90 and Ki67 IHC staining in Veh- and Rapa-treated mouse livers. Scale bar: 100 μm (H&E); 100 μm (IHC). (E) Representative Western blotting from Veh and Rapa liver tissues. Arrows on the left side of the blots indicate the correct band for the indicated proteins. **P* < 0.05, ***P* < 0.01, ****P* < 0.001, and *****P* < 0.0001. HCC, hepatocellular carcinoma; Pre, pre-treatment; Veh, vehicle; Rapa, rapamycin; H&E, hematoxylin and eosin; IHC, immunohistochemical; GAPDH, glyceraldehyde-3-phosphate dehydrogenase.

The liver-to-body weight ratio, often used to evaluate tumor burden, was significantly reduced in the rapamycin-treated group compared with the vehicle group ($P < 0.05$; Fig. 2B and C). H&E staining revealed that rapamycin markedly reduced tumor formation in liver tissues compared with the vehicle group. IHC analysis indicated a significant decrease in the proportion of Ki-67–positive cells in liver tissues following rapamycin administration ($P < 0.05$; Fig. 2D). In addition, Western blot analysis showed that rapamycin significantly downregulated the protein expression levels of p-mTOR, p-RPS6, Ccnd1, FTH1, SLC7A11, and GPX4 in liver tissues compared with the vehicle group ($P < 0.05$), whereas p-4EBP1 (T37/46) and p-4EBP1 (Ser65) showed only a non-significant decreasing trend ($P > 0.05$; Fig. 2E). Collectively, these results further demonstrate that rapamycin exerts its anti-proliferative effects predominantly through inhibition of the mTOR/RPS6 signaling axis, while exerting a comparatively modest effect on the mTOR/4EBP1 pathway. Moreover, rapamycin promotes ferroptosis in HCC tumor tissues.

4EBP1A4 delays HCC progression

Given the significant role of 4EBP1 phosphorylation in mTOR-mediated tumor progression, MHCC97H and SNU449 cells were transfected with pCMV-4EBP1WT or pCMV-4EBP1A4 plasmids. The results showed that, compared with the 4EBP1WT group, the 4EBP1A4 mutant significantly reduced cell viability and increased cell death ($P < 0.05$; Fig. 3A and B; Supplementary Fig. 2A and B). The protein levels of p-4EBP1 (T37/46) and p-4EBP1 (Ser65) in the 4EBP1A4 group were significantly lower than those in the 4EBP1WT group, and the expression of proliferation-related proteins, including Ccnd1 and PCNA, was also markedly decreased ($P < 0.05$; Fig. 3C; Supplementary Fig. 2C). Furthermore, ferroptosis-related biomarkers showed clear differences between the two groups. Compared with 4EBP1WT cells, 4EBP1A4 significantly reduced the expression of SLC7A11, FTH1, and GPX4, while increasing ACSL4 levels ($P < 0.05$; Fig. 3D; Supplementary Fig. 2D). A significant reduction in the GSH/GSSG ratio was observed

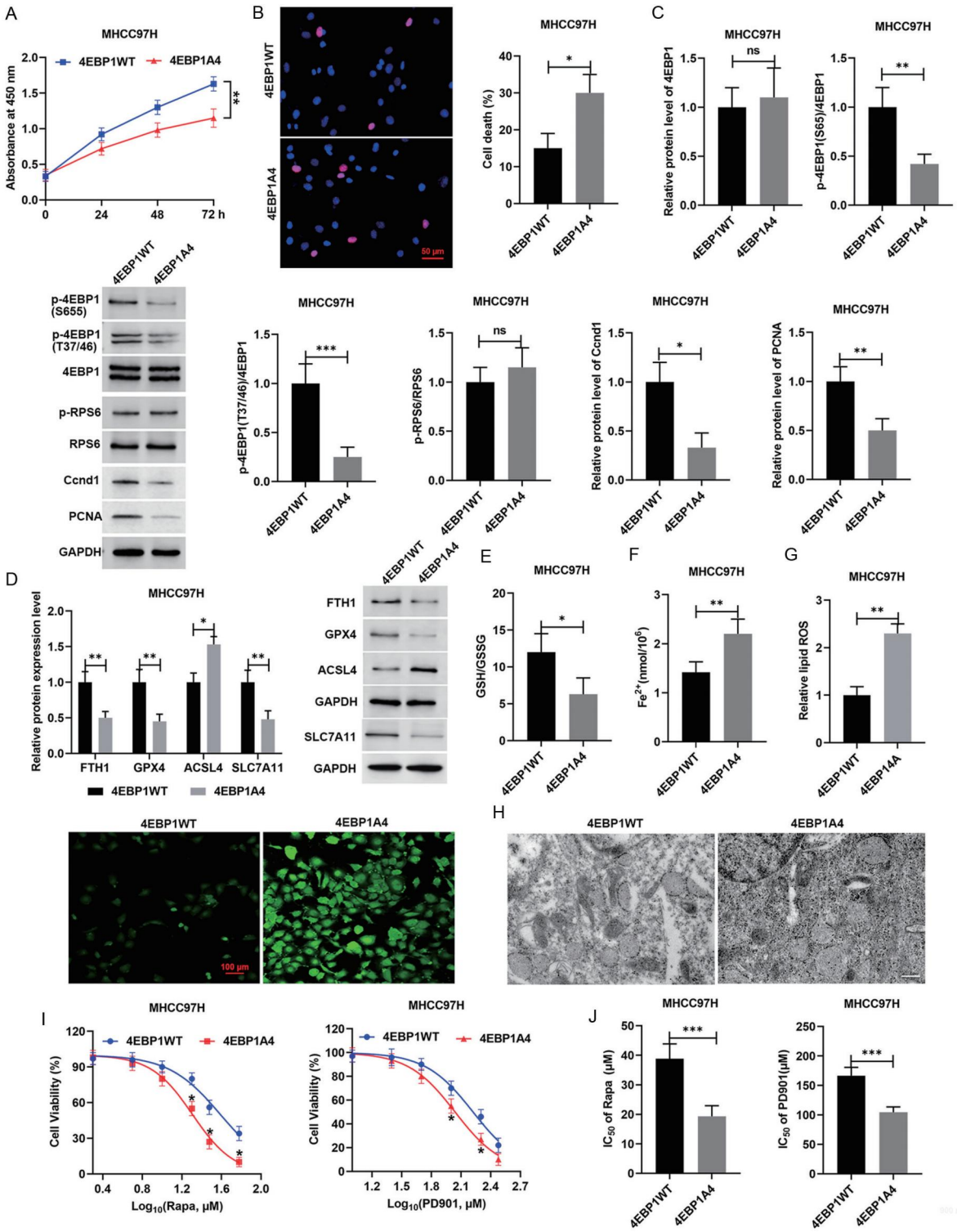

Fig. 3. The regulatory effects of 4EBP1A4 on rapamycin-induced ferroptosis in HCC cells. (A) Cell viability was assessed by CCK-8 assay. (B) Cell death was detected by PI staining (Scale bar: 50 μm). (C) mTOR pathway- and proliferation-associated proteins were detected by Western blot assay. (D) Ferroptosis-associated protein levels were detected by Western blot assay. (E) The ratio of GSH/GSSG was detected using the GSH and GSSG Assay Kit. (F) Intracellular Fe^{2+} levels were measured using an iron assay kit. (G) The level of lipid ROS in HCC cells was detected using a C11-BODIPY 581/591 lipid peroxidation detection kit (Scale bar: 100 μm). (H) Mitochondrial ultrastructure was observed by TEM (Scale bar: 900 nm). (I, J) The cytotoxic effects of rapamycin and PD901 on HCC cells were evaluated using the CCK-8 assay. Cells were treated with rapamycin (2, 5, 10, 20, 40, and 60 μM) and PD901 (10, 25, 50, 100, 200, and 300 μM). IC50 values for rapamycin and PD901 were calculated based on dose–response curves. Each experiment was performed in triplicate. *$P < 0.05$, **$P < 0.01$, ***$P < 0.001$. HCC, hepatocellular carcinoma; PI, propidium iodide; CCK-8, Cell Counting Kit-8; ROS, reactive oxygen species; TEM, transmission electron microscopy; GAPDH, glyceraldehyde-3-phosphate dehydrogenase.

in 4EBP1A4 cells, accompanied by increased intracellular lipid ROS and Fe^{2+} accumulation ($P < 0.05$; Fig. 3E–G; Supplementary Fig. 2E–G). Additionally, 4EBP1A4 cells exhibited ferroptosis-associated morphological alterations, including mitochondrial shrinkage and reduced or absent cristae (Fig. 3H). Moreover, following treatment with varying concentrations of rapamycin and PD901, both the 4EBP1WT and 4EBP1A4 groups showed concentration-dependent reductions in cell viability, with a more pronounced effect observed in the 4EBP1A4 group ($P < 0.05$; Fig. 3I–J; Supplementary Fig. 2H and I). Notably, ferrostatin-1 (5 μM, 24 h) reversed the 4EBP1A4-mediated inhibition of cell viability and ferroptosis ($P < 0.05$; Supplementary Fig. 3A–F). Collectively, these results indicate that 4EBP1A4 induces ferroptosis and inhibits tumor cell proliferation. Importantly, 4EBP1A4 sensitizes tumor cells to rapamycin and PD901.

Subsequently, the c-Met/β-cateninΔN90/4EBP1A4 plasmid was hydrodynamically injected into the tail vein of mice for *in vivo* validation, and rapamycin treatment was initiated 4.7 weeks post-injection (Fig. 4A). The results demonstrated a significant reduction in tumor burden in the rapamycin-treated group compared with the vehicle group ($P < 0.05$; Fig. 4B and C). Moreover, the combination of 4EBP1A4 and rapamycin demonstrated superior efficacy in suppressing tumor growth compared with rapamycin monotherapy ($P < 0.05$; Fig. 4D). Tumor nodules were observed in liver tissues from the pre-treatment, vehicle, and rapamycin groups, as confirmed by H&E staining. IHC analysis revealed high β-catenin expression in tumor tissues, and Ki-67 staining indicated that rapamycin significantly inhibited tumor cell proliferation compared with the vehicle group ($P < 0.05$; Fig. 4E). Western blot analysis showed significantly lower protein expression levels of p-mTOR, p-RPS6, Ccnd1, PCNA, SLC7A11, FTH1, and GPX4 in liver tissues from the rapamycin-treated group compared with the vehicle group ($P < 0.05$; Fig. 4F). Additionally, rapamycin significantly decreased the hepatic GSH/GSSG ratio while increasing lipid ROS and Fe^{2+} levels compared with the vehicle group ($P < 0.05$; Fig. 4G–I). Collectively, these findings indicate that 4EBP1A4 promotes ferroptosis, thereby enhancing the therapeutic efficacy of rapamycin.

Non-phosphorylated 4EBP1 drives Nrf2 ubiquitination and degradation

Subsequently, the molecular mechanisms underlying 4EBP1-mediated ferroptosis regulation were investigated. HSP90β, a molecular chaperone known to stabilize multiple client proteins, has been implicated in malignant tumor progression.[26] Prediction using the HitPredict database suggested a potential protein–protein interaction between 4EBP1 and HSP90β. Subsequently, Co-IP and immunofluorescence colocalization analyses further validated the physical interaction between 4EBP1 and HSP90β, while the 4EBP1D4 mutant exhibited significantly reduced binding capacity (Fig. 5A and B). Notably, 4EBP1A4 prevented Keap1 from interacting with HSP90β (Fig. 5C). As a substrate-specific adaptor of the BTB-CUL3-RBX1 E3 ubiquitin ligase complex, Keap1 mediates Nrf2 ubiquitination and subsequent degradation through direct binding.[27] In this study, HSP90β overexpression significantly increased Nrf2 protein levels in HCC cells (Fig. 5D). Subsequently, treatment with the proteasome inhibitor MG132 abolished Nrf2 downregulation, suggesting involvement of the ubiquitin–proteasome pathway (Fig. 5E). Further investigation revealed that HSP90β overexpression attenuated Nrf2 ubiquitination, primarily through K48-linked polyubiquitin chains (Fig. 5F and G). Cycloheximide chase experiments showed that HSP90β silencing significantly shortened Nrf2 protein half-life (Fig. 5H and I). Immunofluorescence analysis further showed that HSP90β upregulation enhanced Nrf2 accumulation and promoted its nuclear translocation (Fig. 5J). Additionally, Western blot analysis showed unchanged expression of HSP90β and Keap1 in 4EBP1A4-expressing cells, whereas Nrf2 protein levels were markedly reduced (Fig. 5K). Collectively, these findings suggest that 4EBP1A4 competitively binds HSP90β with Keap1, thereby promoting Keap1-mediated K48-linked ubiquitination and degradation of Nrf2. This leads to reduced Nrf2 nuclear translocation and increased intracellular ROS levels, ultimately enhancing ferroptosis.

HSP90β overexpression reverses 4EBP1A4-induced ferroptosis activation and proliferative inhibition in HCC cells

To validate the role of HSP90β in 4EBP1-regulated ferroptosis, HSP90β was overexpressed in 4EBP1A4 mutant cells. The results demonstrated that, compared with the vector group, 4EBP1A4 significantly suppressed cell viability, increased cell death, and downregulated proliferation-related proteins (including Ccnd1 and PCNA). Notably, HSP90β overexpression effectively reversed these effects induced by 4EBP1A4 ($P < 0.05$; Fig. 6A–C; Supplementary Fig. 4A–C). Compared with the vector group, 4EBP1A4 significantly downregulated ferroptosis-related proteins SLC7A11, FTH1, and GPX4 ($P < 0.05$; Fig. 6D; Supplementary Fig. 4D), decreased the intracellular GSH/GSSG ratio and ΔΨm, and increased lipid ROS and Fe^{2+} levels ($P < 0.05$; Fig. 6E–H; Supplementary Fig. 4E–H). Furthermore, 4EBP1A4 induced characteristic mitochondrial morphological alterations, including mitochondrial shrinkage and reduced or absent cristae (Fig. 6I). Similarly, HSP90β overexpression reversed 4EBP1A4-mediated ferroptosis activation. These findings provide strong evidence that HSP90β serves as a key mediator in 4EBP1-regulated ferroptosis, and that 4EBP1A4 overcomes ferroptosis resistance through the HSP90β/Keap1/Nrf2 pathway.

Synergistic targeting of the mTOR and ERK pathways suppresses β-catenin-mutant HCC

This study assessed antitumor efficacy in SNU449 and MHCC97H cells using mTOR inhibitors (rapamycin, MLN0128), an MEK inhibitor (PD901), and their combination (Comb: MLN0128 + PD901). The results demonstrated that all four treatment regimens significantly increased cell death, with MLN0128 showing superior efficacy compared with rapamycin, while the combination treatment showed maximal growth inhibition ($P < 0.05$; Fig. 7A; Supplementary Fig. 5A). Both rapamycin and MLN0128 significantly reduced the expression levels of p-mTOR, p-RPS6, p-4EBP1 (T37/46), and p-4EBP1 (Ser65), with MLN0128 showing greater efficacy. PD901 treatment effectively suppressed p-ERK and both 4EBP1 phosphorylation sites, while the combination therapy produced maximal pathway inhibition ($P < 0.05$; Fig. 7B; Supplementary Fig. 5B). Furthermore, all four treatment regimens significantly downregulated Ccnd1, PCNA, and Nrf2 protein expression ($P < 0.05$; Fig. 7C and D; Supplementary Fig. 5C and D). In the assessment of ferroptosis-related indicators, all treatments significantly decreased the GSH/GSSG ratio and ΔΨm, while increasing Fe^{2+} levels ($P < 0.05$; Fig. 7E–G; Supplementary Fig. 5E–G). Collectively, these results indicate that rapamycin, MLN0128, PD901, and their combinations induce ferroptosis and inhibit tumor growth, with combination therapy showing superior efficacy.

Subsequently, the therapeutic efficacy of rapamycin, MLN0128, PD901, and the combination was further validated through animal experiments (Fig. 8A). Post-treatment analysis revealed tumor nodules in liver tissues across all experi-

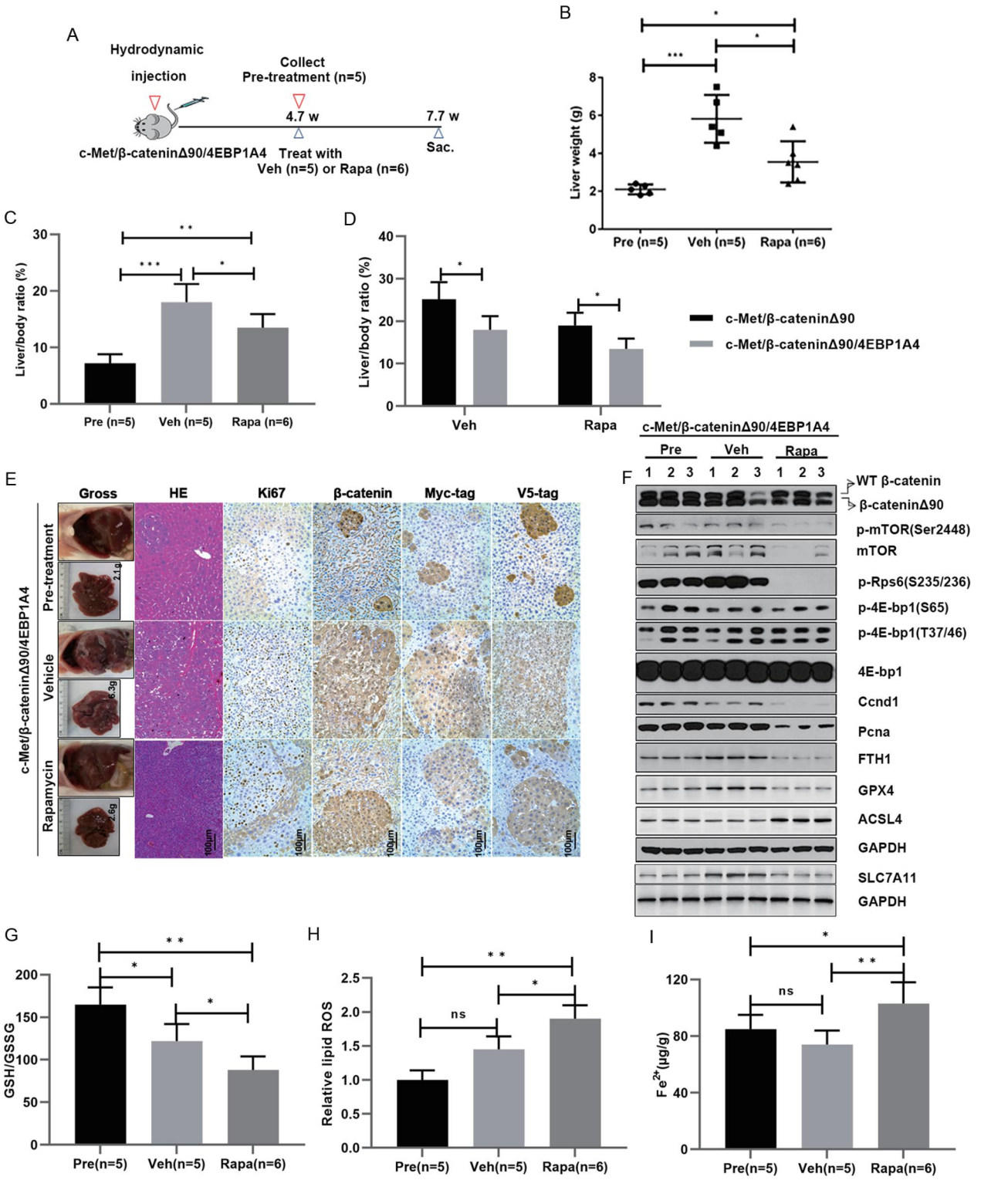

Fig. 4. Effects of 4EBP1A4 on the therapeutic efficacy of rapamycin. (A) Study design. (B, C) Liver weight and liver/body ratio of c-Met/β-cateninΔ90/4EBP1A4-injected mice treated with Pre, Veh, and Rapa. (D) Tumor burden after hydrodynamic injection of c-Met/β-cateninΔ90/4EBP1A4 or c-Met/β-cateninΔ90. (E) Gross, H&E images, and IHC staining of β-cateninΔ90, β-catenin, and Ki67 in Pre-, Veh-, and Rapa-treated mouse livers. Scale bar: 100 μm (H&E); 100 μm (IHC). (F) Representative Western blotting from Pre, Veh, and Rapa liver tissues. Arrows on the left side of the blots indicate the correct band for the indicated proteins. (G) The ratio of GSH/GSSG was detected using the GSH and GSSG Assay Kit. (H) Detection of lipid ROS levels in liver tissues using C11-BODIPY 581/591 kit. I. Fe^{2+} levels in liver tissues were measured using an iron assay kit. **P* < 0.05, ***P* < 0.01, and ****P* < 0.001. Pre, pre-treatment; Veh, vehicle; Rapa, rapamycin; H&E, hematoxylin and eosin; IHC, immunohistochemical; ROS, reactive oxygen species; GAPDH, glyceraldehyde-3-phosphate dehydrogenase.

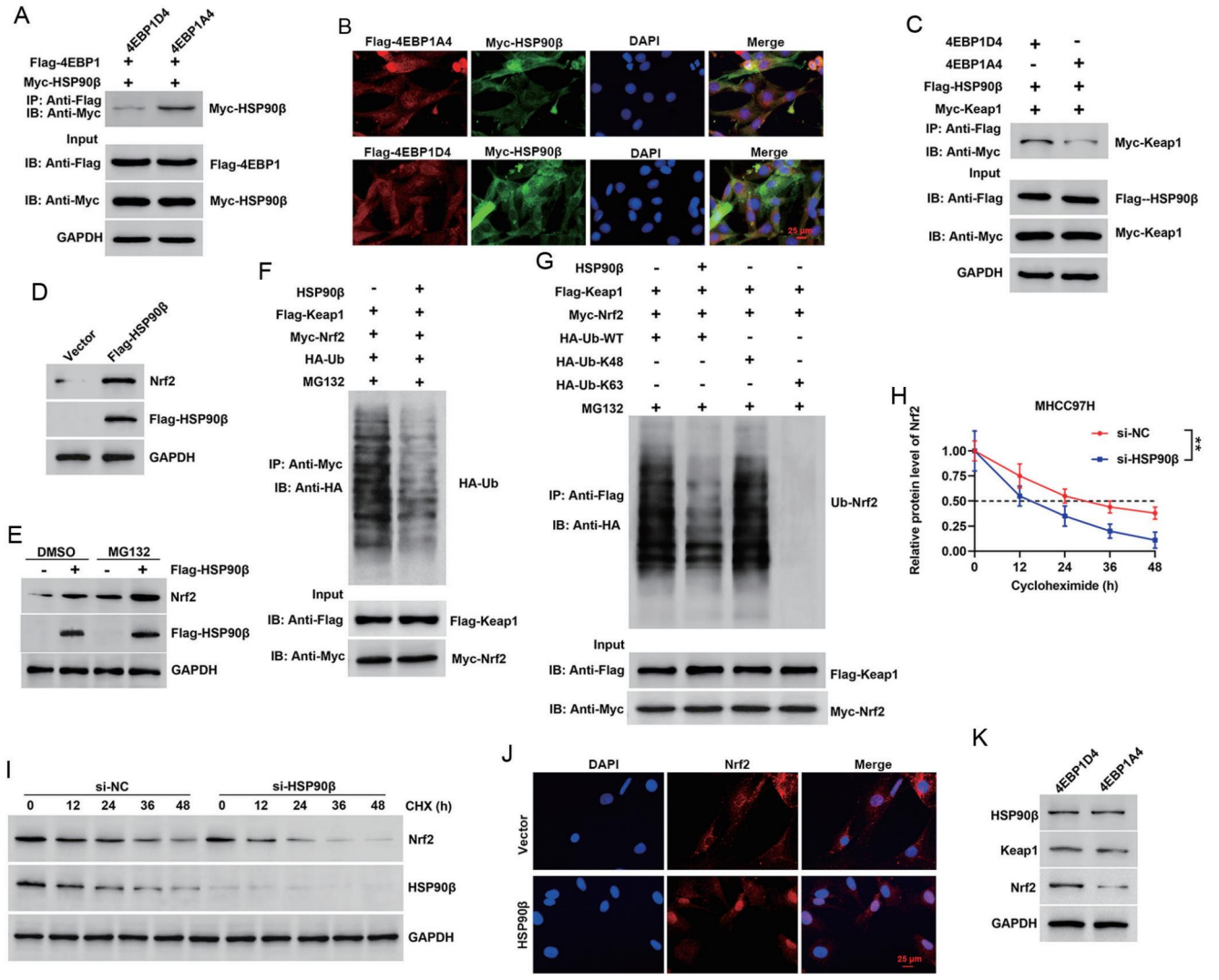

Fig. 5. Analysis of 4EBP1A4 regulation of ferroptosis via the HSP90β/Keap1/Nrf2 pathway. (A) The interaction between 4EBP1 and HSP90β was detected by co-IP assay in MHCC97H cells. (B) Immunofluorescence analysis of co-localization of 4EBP1 and HSP90β in HCC cells. Scale bar: 25 μm. (C) The effect of 4EBP1 phosphorylation status on the HSP90β–Keap1 interaction was assessed by co-IP. (D) Nrf2 protein expression in HCC cells transfected with Flag-HSP90β was detected by Western blotting. (E) The effect of MG132 (10 μM) on Nrf2 expression in Flag-HSP90β-transfected HCC cells was assessed. (F, G) HCC cells transfected with pcDNA3.1-HSP90β, Flag-Keap1, Myc-Nrf2, and HA-Ub were treated with MG132 (20 μM) for 24 h. Co-IP and Western blotting were used to detect ubiquitination levels of Nrf2. (H, I) The half-life of Nrf2 regulated by HSP90β was analyzed by Western blotting. HCC cells were transfected with si-NC or si-HSP90β for 48 h and then exposed to 100 μg/mL CHX for 0, 12, 24, and 48 h. The intensity of Nrf2 expression for each band was normalized to that of GAPDH. (J) Immunofluorescence staining was performed to examine the effect of HSP90β on Nrf2 nuclear localization. Scale bar: 25 μm. K. Nrf2, Keap1, and HSP90β protein levels were assessed via Western blot assay. ***P* < 0.01. co-IP, co-immunoprecipitation; HCC, hepatocellular carcinoma; CHX, cycloheximide. +, cells transfected with the indicated tagged protein; -, cells were not transfected with the indicated tagged protein; GAPDH, glyceraldehyde-3-phosphate dehydrogenase.

mental groups (pre-treatment, vehicle, rapamycin, MLN0128 [0.5 mg/kg], MLN0128 [1.0 mg/kg], PD901, and combination). The combination group showed the most significant tumor reduction, with markedly fewer nodules than other groups. Tumor lesions were also observed via H&E staining. Compared with the vehicle group, all drug treatments significantly reduced liver weight and inhibited tumor growth ($P < 0.05$; Fig. 8B–D). Additionally, IHC results revealed high expression of β-cateninΔN90 in tumor regions. Compared with the vehicle group, all five drug treatments significantly decreased the proportion of Ki-67–positive cells in liver tissues ($P < 0.05$; Fig. 8B and 8E). The combination treatment markedly inhibited tumor cell proliferation. Western blot analysis showed that, compared with the vehicle group, expression of p-4EBP1 (T37/46), p-4EBP1 (Ser65), PCNA, Nrf2, FTH1, and GPX4 was significantly downregulated in liver tissues treated with MLN0128 (0.5 mg/kg), PD901, and the combination. PD901 and combination treatments notably suppressed p-ERK (Thr202/Tyr204) expression ($P < 0.05$; Fig. 8F). Compared with the vehicle group, MLN0128, PD901, and combination treatments all significantly reduced hepatic GSH/GSSG ratio and increased lipid ROS and Fe^{2+} levels, with the combination showing the most pronounced effect ($P < 0.05$; Fig. 8G–I). These results further demonstrate that rapamycin, MLN0128, PD901, and the combination inhibited β-catenin-mutant HCC progression via the mTOR and MEK/ERK pathways, with the combination showing the most potent effect. Moreover, MLN0128, PD901, and combination

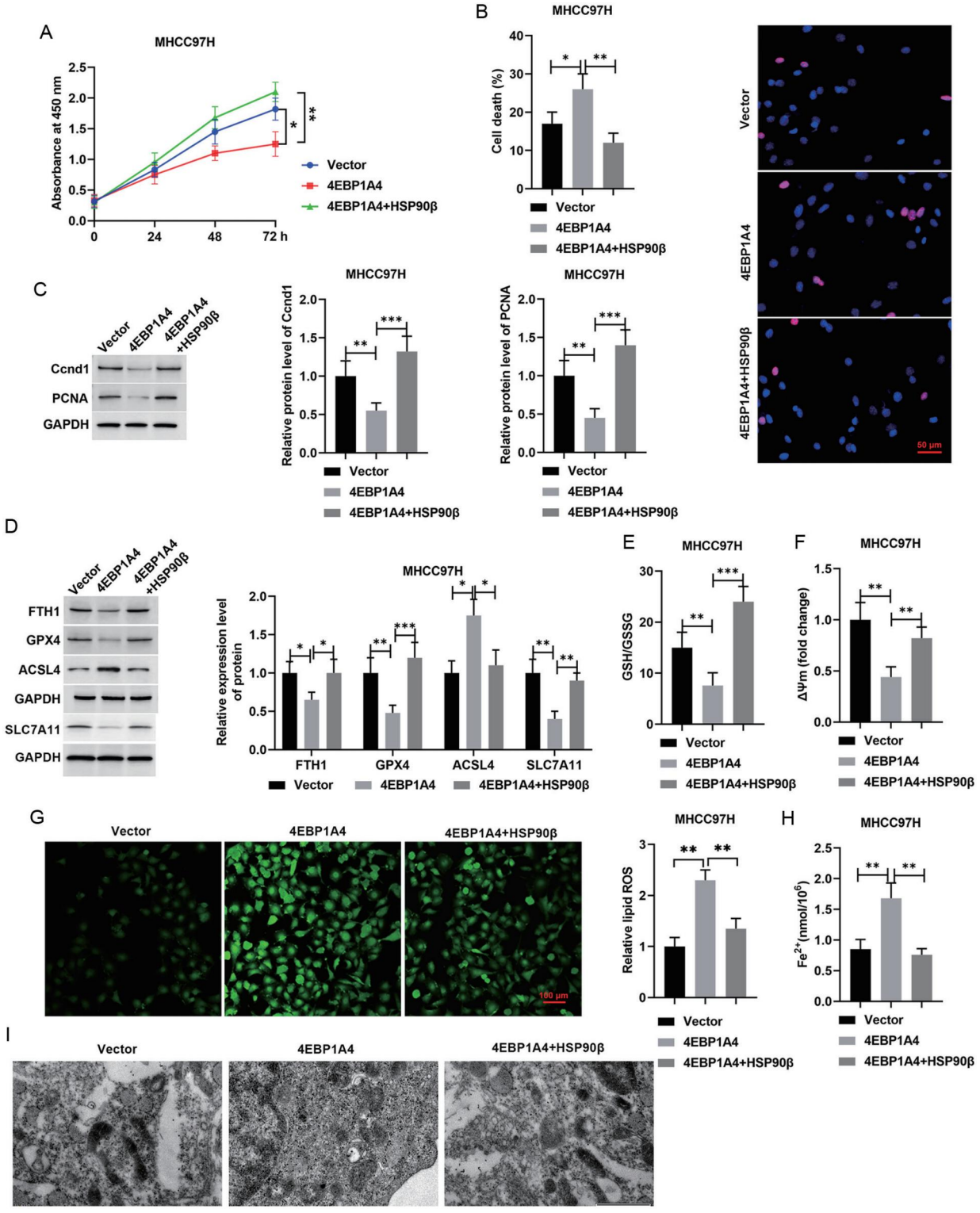

Fig. 6. Effects of HSP90β overexpression on 4EBP1A4- mediated ferroptosis in HCC cells. (A) Cell viability was assessed by CCK-8 assay. (B) Cell death was detected by PI staining (Scale bar: 50 μm). (C) Proliferation-associated proteins were detected by Western blot assay. (D) Ferroptosis-associated protein levels were detected by Western blot assay. (E) The ratio of GSH/GSSG was detected using the GSH and GSSG Assay Kit. (F) Quantification of ΔΨm was performed by JC-1 fluorescence staining. (G) Detection of lipid ROS levels in HCC cells using C11-BODIPY staining (Scale bar: 100 μm). (H) Intracellular Fe^{2+} levels were measured using an iron assay kit. (I) Mitochondrial ultrastructure was visualized by TEM (Scale bar: 200 nm). Each experiment was performed in triplicate. **P* < 0.05, ***P* < 0.01, and ****P* < 0.001. HCC, hepatocellular carcinoma; PI, propidium iodide; CCK-8, Cell Counting Kit-8; ΔΨm, mitochondrial membrane potential; ROS, reactive oxygen species; JC-1, 5,5′,6,6′-tetrachloro-1,1′,3,3′-tetraethylbenzimidazolylcarbocyanine iodide; TEM, transmission electron microscopy; GAPDH, glyceraldehyde-3-phosphate dehydrogenase.

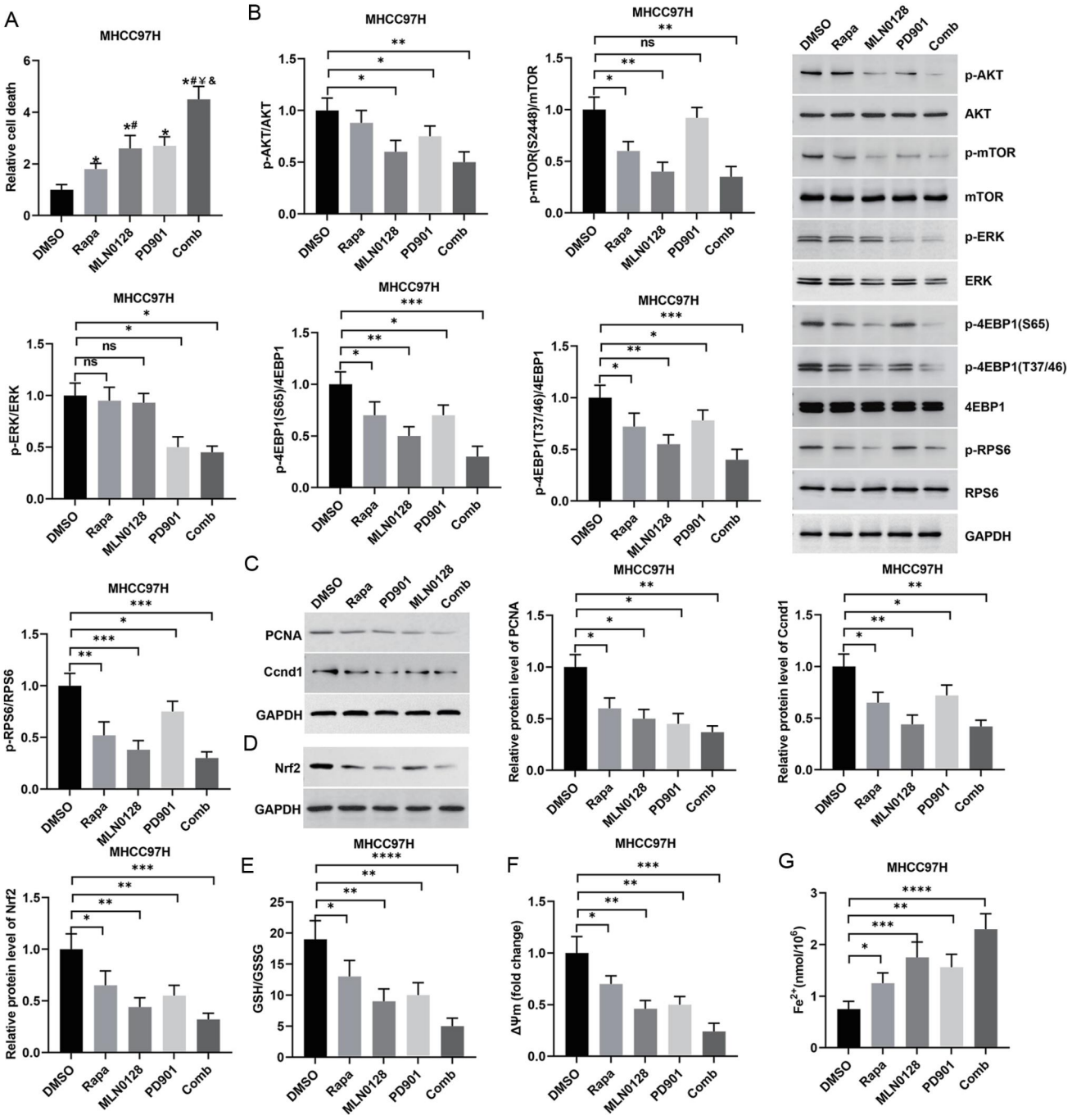

Fig. 7. Effects of combined inhibition of mTOR and ERK pathways on ferroptosis and proliferation in HCC cells. (A) Quantification of cell death ratio following PI staining. (B-D) Protein expression levels of mTOR signaling components, proliferation markers, and Nrf2 were detected by Western blot assay. (E) GSH/GSSG ratio was detected using the GSH and GSSG Assay Kit. (F) Quantification of JC-1 staining for ΔΨm. (G) Intracellular Fe^{2+} levels were measured using an iron assay kit. Each experiment was performed in triplicate. **P* < 0.05, ***P* < 0.01, and ****P* < 0.001. # *P* < 0.05 compared with the Rapa group; ¥ *P* < 0.05 compared with the MLN0128 group; & *P* < 0.05 compared with the PD901 group. DMSO, dimethyl sulfoxide; Rapa, rapamycin; Comb, combination, in which cells were treated with 5 μM MLN0128 plus 150 μM PD901; HCC, hepatocellular carcinoma; PI, propidium iodide; ΔΨm, mitochondrial membrane potential; JC-1, 5,5′,6,6′-tetrachloro-1,1′,3,3′-tetraethylbenzimidazolylcarbocyanine iodide; GAPDH, glyceraldehyde-3-phosphate dehydrogenase.

treatment induced ferroptosis.

Discussion

HCC is a highly prevalent malignant tumor in the global digestive system. Alarmingly, the overall 5-year survival rate of HCC patients remains below 20%.[1] The development of HCC is mainly driven by six key biological processes: cell cycle regulation, epigenetic dysregulation, oxidative stress, activation of the RAS/RAF/MAPK signaling pathway, mainte-

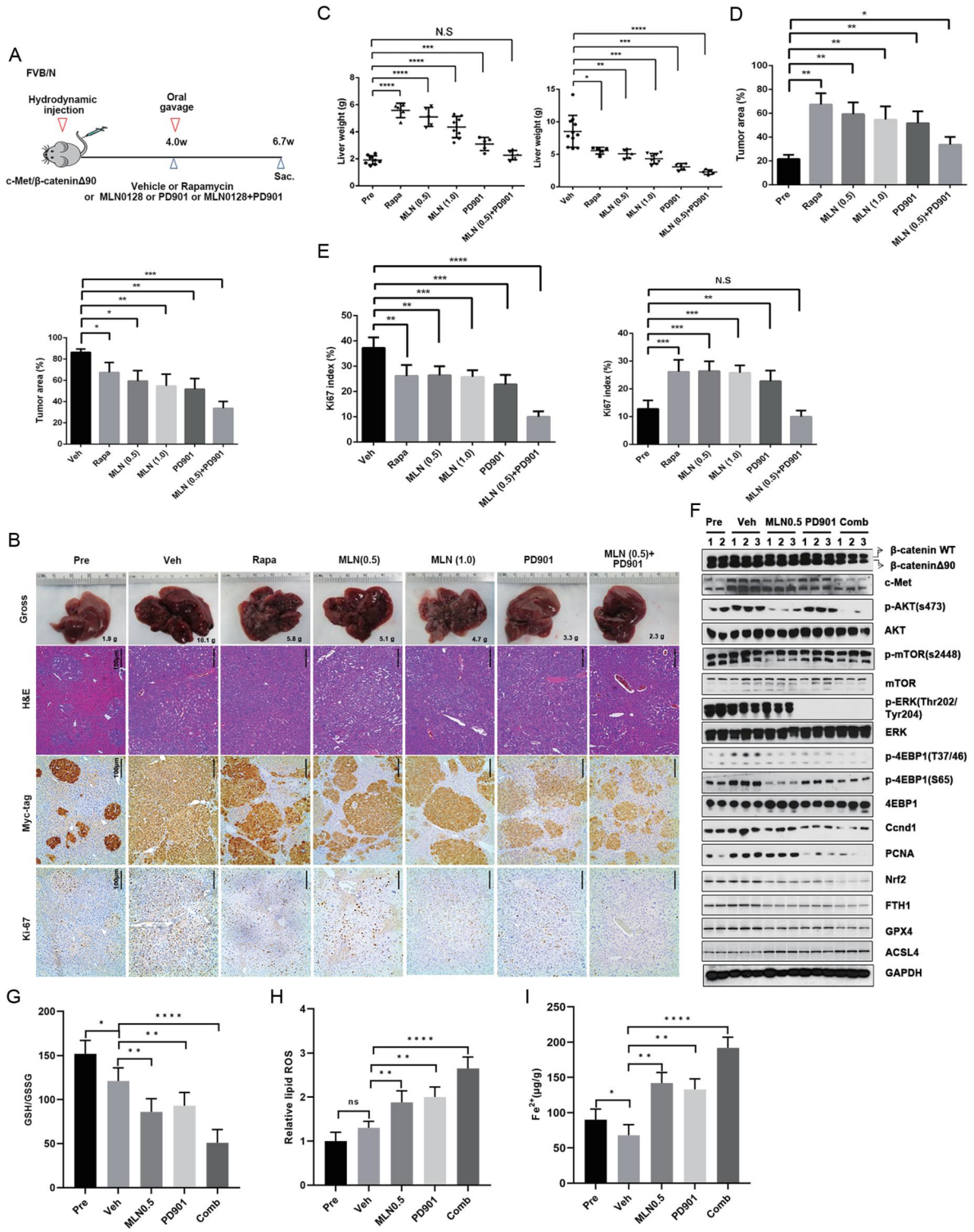

Fig. 8. Analysis of the therapeutic effects of combined mTOR and ERK inhibitors in an HCC mouse model. (A) Study design. (B) Gross, H&E images, and IHC staining of β-cateninΔ90, Myc-tag, and Ki67 in liver tissues from Pre, Veh, Rapa (6 mg/kg), MLN0128 (MLN, 0.5 mg/kg), MLN (1 mg/kg), PD901 (10 mg/kg), and combination (0.5 mg/kg MLN + 10 mg/kg PD901)-treated mice. Scale bar: 100 μm (H&E); 100 μm (IHC). (C) Liver weight. (D) Tumor burden (area ratio of tumor/normal tissue) was calculated based on H&E-stained sections shown in panel B. (E) The proportion of Ki67-positive cells was calculated based on IHC-stained sections shown in panel B. (F) Representative Western blotting from liver tissues. Arrows on the left side of the blots indicate the correct band for the indicated proteins. (G) GSH/GSSG ratio was detected using the GSH and GSSG Assay Kit. (H) Quantification of lipid ROS levels in liver tissues detected by C11-BODIPY staining. (I) Fe^{2+} levels in liver tissues were measured using an iron assay kit. *P < 0.05, **P < 0.01, ***P < 0.001, and ****P < 0.0001. HCC, hepatocellular carcinoma; Pre, pre-treatment; Veh, vehicle; Rapa, rapamycin; Comb, combination; H&E, hematoxylin and eosin; IHC, immunohistochemical; ROS, reactive oxygen species; GAPDH, glyceraldehyde-3-phosphate dehydrogenase.

nance of the Wnt/β-catenin pathway, and activation of the PI3K/AKT/mTOR pathway.[28] Approximately 30% of HCC cases harbor CTNNB1 mutations, which enhance the stability of β-catenin and promote its aberrant accumulation, leading to sustained activation of downstream target genes.[29] Moreover, clinical data indicate that co-activation of the Wnt/β-catenin and AKT/mTOR pathways occurs in about 14.4% of HCC patients, with β-catenin upregulating mTOR activity through multiple mechanisms to synergistically drive tumor progression.[30] Furthermore, our previous research has demonstrated that β-catenin-mutant HCC is dependent on mTOR signaling.[31] Although mTOR-mediated ferroptosis inhibition is known to promote tumor progression,[32] the underlying molecular mechanism remains to be fully elucidated.

The regulatory features of mTORC1 on p70S6K/RPS6 have been thoroughly characterized. It has been clearly shown that activation of mTORC1 promotes protein and lipid synthesis, gene transcription, and cellular metabolism, thus facilitating the growth and proliferation of tumor cells.[33] 4EBP1 is another crucial downstream regulatory factor of mTORC1. A recent study demonstrated that 4EBP1-mediated ferroptosis resistance promotes tumor cell survival and disease progression.[34] This study employed both *in vitro* and *in vivo* experimental approaches to investigate the effects of rapamycin on ferroptosis regulation and its therapeutic efficacy. The results indicated that although rapamycin inhibited phosphorylation of both RPS6 and 4EBP1, the inhibitory effect on 4EBP1 was relatively weaker. This relative insensitivity of 4EBP1 to rapamycin may restrict its therapeutic efficacy. To experimentally validate this conclusion, HCC cells were transfected with 4EBP1WT and 4EBP1A4 plasmids. The findings showed that 4EBP1A4 significantly promoted ferroptosis, reduced the viability and proliferative capacity of tumor cells, and enhanced their sensitivity to rapamycin. The results of animal studies indicated that the 4EBP1A4–rapamycin combination therapy achieved superior tumor reduction compared to rapamycin monotherapy. These findings align with previous reports by Wang *et al*., showing marked suppression of HCC progression with this combinatorial approach.[35] Collectively, 4EBP1-mediated ferroptosis plays a vital role in tumor suppression, and 4EBP1A4 can synergistically enhance the therapeutic efficacy of rapamycin in β-catenin-mutant HCC.

HSP90β, a cytosolic isoform of the heat shock protein HSP90, serves as a critical molecular chaperone that orchestrates protein folding, maturation, and functional activation. HSP90β has been recognized as an essential facilitator in malignant tumor development and progression.[26] Moreover, HSP90β is intricately involved in the regulation of mitochondrial function and activation of the antioxidant defense system. Dysregulation of HSP90β can trigger lipid peroxidation and activation of ferroptosis.[36] Previously, a physical interaction between HSP90β and the Keap1 protein was identified, although the functional consequences for Keap1 activity were not fully characterized.[37] Under normal cellular homeostasis, the Keap1–Nrf2 interaction facilitates constitutive Nrf2 ubiquitination and degradation, thereby tightly maintaining appropriate intracellular Nrf2 protein levels. As a master regulator of antioxidant responses, Nrf2 plays a pivotal role in suppressing ferroptosis. In this study, a physical interaction between 4EBP1 and HSP90β was identified through both HitPredict database prediction and Co-IP assays. Furthermore, competitive binding between 4EBP1A4 and Keap1 to HSP90β was observed. HSP90β overexpression enhanced Nrf2 protein stability and promoted its nuclear translocation. These findings indicate that HSP90β modulates Nrf2 ubiquitination. Co-IP analyses further revealed reduced K48-linked polyubiquitination of Nrf2 in Flag-Keap1 immunoprecipitates from HSP90β-overexpressing cells. CHX-based protein stability analysis confirmed that HSP90β knockdown significantly shortened the half-life of Nrf2. Notably, this study also demonstrated that HSP90β overexpression reversed the 4EBP1A4-mediated suppression of tumor cell viability and induction of ferroptosis. Mechanistically, 4EBP1A4 and Keap1 competitively bind to HSP90β, increasing Keap1–Nrf2 complexes to accelerate Nrf2 degradation and ferroptosis susceptibility, thereby suppressing HCC.

Rapamycin selectively inhibits mTORC1 by binding to the FKBP12-rapamycin binding domain of mTOR but does not directly affect mTORC2. However, mTORC2 can promote mTORC1 activity via AKT phosphorylation. Rapamycin (sirolimus) and its derivatives (temsirolimus, everolimus) are first-generation mTOR inhibitors, which exert only partial inhibition of mTORC1 and fail to target mTORC2, leading to limited efficacy and drug resistance.[38] In contrast, MLN0128 is an ATP-competitive mTOR kinase inhibitor that binds to the catalytic active site of mTOR, thereby suppressing both mTORC1 and mTORC2 activities.[39] Preclinical studies have demonstrated remarkable anti-cancer effects of these inhibitors.[39] This study provides both *in vitro* and *in vivo* evidence that MLN0128 outperforms rapamycin in inhibiting HCC development via ferroptosis induction. Furthermore, ERK signaling activation also limits the therapeutic efficacy of mTOR inhibitors.[40] The MEK/ERK pathway directly phosphorylates Raptor, which leads to enhanced mTORC1 kinase activity. Some studies have also found that ERK directly modulates 4EBP1 phosphorylation status, consequently promoting translation initiation.[11,41] Moreover, ERK stabilizes β-catenin and facilitates its nuclear translocation, creating a positive feedback loop that promotes HCC progression.[42] A study has revealed that aberrant activation of the PI3K/AKT/mTOR signaling pathway occurs in approximately 50% of HCC cases, while overexpression and phosphorylation of MEK and ERK are observed in more than 75% of HCC clinical specimens.[43] Research has also indicated that the combination of MEK and mTOR inhibitors significantly impedes HCC growth both *in vitro* and *in vivo*.[15] Consistent with these findings, this study also revealed constitutive activation of both mTOR and ERK signaling pathways in HCC cells. Therefore, this study further explored the therapeutic effect of combining MLN0128 and PD901. PD901, an ERK inhibitor, directly binds to and inhibits MEK1/2, leading to a marked reduction in p-ERK levels, and has shown antitumor activity across various preclinical cancer models.[44] The results demonstrated that both MLN0128 and PD901 inhibited tumor cell proliferation by suppressing the mTOR signaling pathway. Notably, compared to monotherapy, the combination synergistically enhanced ferroptosis, effectively blocked mTOR signaling pathway compensation, and consequently improved the therapeutic effect on β-catenin-mutant HCC.

In the treatment of advanced HCC, mTOR inhibitor-based immunosuppressive regimens (e.g., everolimus, sirolimus/rapamycin) play a critical role in preventing HCC recurrence after liver transplantation. However, the lack of reliable biomarkers and the emergence of acquired resistance remain major clinical challenges. Thus, elucidating resistance mechanisms and developing effective combination strategies are essential to improve the clinical benefit of mTOR inhibitors in HCC. This study offers new insights: first, we found that p-4EBP1 levels correlate closely with rapamycin sensitivity, suggesting that p-4EBP1 expression in tumor tissues could serve as a biomarker to identify susceptible patients and enable stratification. Second, MLN0128 exhibited superior anti-HCC efficacy than rapamycin, supporting the development of improved mTOR inhibitors. Furthermore, combined

inhibition of the mTOR and ERK pathways synergistically induced ferroptosis and blocked compensatory pathway activation, thereby effectively suppressing HCC progression. This combination strategy provides a novel rationale and potential therapeutic avenue to overcome acquired resistance to mTOR inhibitors and to enhance second-line treatment outcomes in advanced HCC.

Nevertheless, certain limitations remain in this study: 1) The effect of 4EBP1 expression modulation on the combination therapy of MEK and mTOR inhibitors was not investigated. 2) Although the results demonstrated that combining 4EBP1A4 with rapamycin, or MLN0128 with PD901, significantly enhances HCC treatment efficacy, the potential toxicities and adverse effects of these combinations remain undetermined. Consequently, it is imperative to further investigate the efficacy of 4EBP1 in combination therapies involving mTOR inhibitors and other pharmacological agents, while also assessing potential adverse effects, thereby providing novel insights and evidence-based foundations for clinical treatment strategies in HCC.

Conclusions

Activation of mTOR (mTORC1 and mTORC2) and ERK signaling inhibits ferroptosis by increasing 4EBP1 phosphorylation, thereby promoting β-catenin-mutant HCC progression. This study demonstrates that 4EBP1A4 and Keap1 competitively bind to HSP90β, increasing Keap1–Nrf2 complexes to accelerate Nrf2 degradation, thereby relieving mTORC1 activation-mediated ferroptosis inhibition (as illustrated in the graphical abstract). Additionally, 4EBP1 serves as a critical downstream effector common to both ERK and mTOR pathways. The combination therapy of MLN0128 and PD901 not only effectively suppresses mTOR compensatory activation but also synergistically induces ferroptosis, leading to significantly improved therapeutic efficacy against β-catenin-mutant HCC. This study provides novel insights for advancing therapeutic strategies and targeted drug development in HCC.

Supporting information

Supplementary material for this article is available at https://doi.org/10.14218/JCTH.2026.00072.

Funding

This study was supported by the Youth Program of the National Natural Science Foundation of China (81902449), the Youth Program of the National Natural Science Foundation of China (82203082), the Shaanxi Provincial Key Research and Development Program (2024SF-YBXM-048), and the Basic Funding for Central Universities (China, xzy012023116).

Conflict of interest

The authors have no conflict of interests related to this publication.

Author contributions

Conceptualization (RL, YZ, NW, RS, MX), investigation (RL, YZ), methodology (RL, YZ, ZW, GL), writing - original draft (RL, YZ), supervision (NW, RS, MX), writing - review and editing (NW, RS, MX), software (ZW, GL, DF, LH, FD), visualization (ZW, GL), resources (DF, LH, FD), validation (DF, LH, FD), and data curation (DF, LH, FD). All authors have approved the final version and publication of the manuscript.

Ethical statement

This research was approved by the Ethics Committee of Xi'an Jiaotong University (approval number: XJTUAE2025-1165). All animal experiments were conducted in accordance with the Guide for the Care and Use of Laboratory Animals established by the United States National Institutes of Health (Bethesda, MD, USA). All animals received human care.

Data sharing statement

The data that support the findings of this study are available from the corresponding author upon reasonable request.

References

[1] Chidambaranathan-Reghupaty S, Fisher PB, Sarkar D. Hepatocellular carcinoma (HCC): Epidemiology, etiology and molecular classification. Adv Cancer Res 2021;149:1–61. doi:10.1016/bs.acr.2020.10.001, PMID:33579421.
[2] Jin H, Qin S, He J, Xiao J, Li Q, Mao Y, *et al*. New insights into checkpoint inhibitor immunotherapy and its combined therapies in hepatocellular carcinoma: from mechanisms to clinical trials. Int J Biol Sci 2022;18(7):2775–2794. doi:10.7150/ijbs.70691, PMID:35541908.
[3] Zhang TQ, Geng ZJ, Zuo MX, Li JB, Huang JH, Huang ZL, *et al*. Camrelizumab (a PD-1 inhibitor) plus apatinib (an VEGFR-2 inhibitor) and hepatic artery infusion chemotherapy for hepatocellular carcinoma in Barcelona Clinic Liver Cancer stage C (TRIPLET): a phase II study. Signal Transduct Target Ther 2023;8(1):413. doi:10.1038/s41392-023-01663-6, PMID:37884523.
[4] Cheng AL, Hsu C, Chan SL, Choo SP, Kudo M. Challenges of combination therapy with immune checkpoint inhibitors for hepatocellular carcinoma. J Hepatol 2020;72(2):307–319. doi:10.1016/j.jhep.2019.09.025, PMID:31954494.
[5] Pan S, Wang J, Tian J, Wang Y, Wang S, Yu Y, *et al*. Safety and efficacy of PD-1 inhibitors plus tyrosine kinase inhibitors combination therapy in patients with advanced hepatocellular carcinoma combined with hyperbilirubinemia: a retrospective cohort study. Front Immunol 2025;16:1530477. doi:10.3389/fimmu.2025.1530477, PMID:40134422.
[6] Zhan M, Ding Y, Huang S, Liu Y, Xiao J, Yu H, *et al*. Lysyl oxidase-like 3 restrains mitochondrial ferroptosis to promote liver cancer chemoresistance by stabilizing dihydroorotate dehydrogenase. Nat Commun 2023;14(1):3123. doi:10.1038/s41467-023-38753-6, PMID:37253718.
[7] Li Y, Yang W, Zheng Y, Dai W, Ji J, Wu L, *et al*. Targeting fatty acid synthase modulates sensitivity of hepatocellular carcinoma to sorafenib via ferroptosis. J Exp Clin Cancer Res 2023;42(1):6. doi:10.1186/s13046-022-02567-z, PMID:36604718.
[8] Wu C, Zhong R, Wei T, Jin Y, He C, Li H, *et al*. Mechanism of targeting the mTOR pathway to regulate ferroptosis in NSCLC with different EGFR mutations. Oncol Lett 2024;28(1):298. doi:10.3892/ol.2024.14431, PMID:38751752.
[9] Fan Y, Ren X, Wang Y, Xu E, Wang S, Ge R, *et al*. Metformin inhibits the proliferation of canine mammary gland tumor cells through the AMPK/AKT/mTOR signaling pathway in vitro. Oncol Lett 2021;22(6):852. doi:10.3892/ol.2021.13113, PMID:34733370.
[10] Yu G, Chen L, Hu Y, Yuan Z, Luo Y, Xiong Y. Antitumor Effects of Baicalein and Its Mechanism via TGFβ Pathway in Cervical Cancer HeLa Cells. Evid Based Complement Alternat Med 2021;2021:5527190. doi:10.1155/2021/5527190, PMID:33777154.
[11] Cohen JD, Gard JM, Nagle RB, Dietrich JD, Monks TJ, Lau SS. ERK crosstalks with 4EBP1 to activate cyclin D1 translation during quinol-thioether-induced tuberous sclerosis renal cell carcinoma. Toxicol Sci 2011;124(1):75–87. doi:10.1093/toxsci/kfr203, PMID:21813464.
[12] Zhuang Q, Zhou T, He C, Zhang S, Qiu Y, Luo B, *et al*. Protein phosphatase 2A-B55δ enhances chemotherapy sensitivity of human hepatocellular carcinoma under the regulation of microRNA-133b. J Exp Clin Cancer Res 2016;35:67. doi:10.1186/s13046-016-0341-z, PMID:27074866.
[13] Velásquez C, Cheng E, Shuda M, Lee-Oesterreich PJ, Pogge von Strandmann L, Gritsenko MA, *et al*. Mitotic protein kinase CDK1 phosphorylation of mRNA translation regulator 4E-BP1 Ser83 may contribute to cell transformation. Proc Natl Acad Sci U S A 2016;113(30):8466–8471. doi:10.1073/pnas.1607768113, PMID:27402756.
[14] Che L, Wu JS, Du ZB, He YQ, Yang L, Lin JX, *et al*. Targeting Mitochondrial COX-2 Enhances Chemosensitivity via Drp1-Dependent Remodeling of Mitochondrial Dynamics in Hepatocellular Carcinoma. Cancers (Basel) 2022;14(3):821. doi:10.3390/cancers14030821, PMID:35159089.
[15] Liu X, Hu J, Song X, Utpatel K, Zhang Y, Wang P, *et al*. Combined Treatment with MEK and mTOR Inhibitors is Effective in In Vitro and In Vivo Models of Hepatocellular Carcinoma. Cancers (Basel) 2019;11(7):930. doi:10.3390/cancers11070930, PMID:31277283.
[16] Jin Y, Rao K, Zheng J, Zhang X, Luo Y, He J. Deficiency of TET2-mediated KMT2D self-transcription confers a targetable vulnerability in hepatocellular carcinoma. PNAS Nexus 2024;3(11):pgae504. doi:10.1093/pnasnexus/pgae504, PMID:39564571.
[17] Hu X, Zhang P, Li S, Zhang J, Wang D, Wang Z, *et al*. Mitochondrial GC-

N5L1 acts as a novel regulator for iron homeostasis to promote sorafenib sensitivity in hepatocellular carcinoma. J Transl Med 2024;22(1):593. doi:10.1186/s12967-024-05404-3, PMID:38918793.
[18] Li S, Yang X, Gao H, Hu X, Wang D, Zhang Q, *et al*. Inhibiting SSBP1 enhances ferroptosis and improves the effectiveness of sorafenib treatment for liver cancer. Int J Oncol 2025;67(3):72. doi:10.3892/ijo.2025.5778, PMID:40747667.
[19] Radenkovic S, Konjevic G, Gavrilovic D, Stojanovic-Rundic S, Plesinac-Karapandzic V, Stevanovic P, *et al*. pSTAT3 expression associated with survival and mammographic density of breast cancer patients. Pathol Res Pract 2019;215(2):366–372. doi:10.1016/j.prp.2018.12.023, PMID:30598340.
[20] Xia P, Zhang H, Lu H, Xu K, Jiang X, Jiang Y, *et al*. METTL5 stabilizes c-Myc by facilitating USP5 translation to reprogram glucose metabolism and promote hepatocellular carcinoma progression. Cancer Commun (Lond) 2023;43(3):338–364. doi:10.1002/cac2.12403, PMID:36602428.
[21] Li A, Xie J, Lv L, Zheng Z, Yang W, Zhuo W, *et al*. RPL9 acts as an oncogene by shuttling miRNAs through exosomes in human hepatocellular carcinoma cells. Int J Oncol 2024;64(6):58. doi:10.3892/ijo.2024.5646, PMID:38639179.
[22] Tao W, Tuo Z, Wu F, Mu K, Xu C, Shi Y, *et al*. Albumin-assembled copper-bismuth bimetallic sulfide bioactive nanosphere as an amplifier of oxidative stress for enhanced radio-chemodynamic combination therapy. Regen Biomater 2022;9:rbac045. doi:10.1093/rb/rbac045, PMID:35855112.
[23] Xu Y, Zhang N, Chen C, Xu X, Luo A, Yan Y, *et al*. Sevoflurane Induces Ferroptosis of Glioma Cells Through Activating the ATF4-CHAC1 Pathway. Front Oncol 2022;12:859621. doi:10.3389/fonc.2022.859621, PMID:35372041.
[24] Qiao Y, Xu M, Tao J, Che L, Cigliano A, Monga SP, *et al*. Oncogenic potential of N-terminal deletion and S45Y mutant β-catenin in promoting hepatocellular carcinoma development in mice. BMC Cancer 2018;18(1):1093. doi:10.1186/s12885-018-4870-z, PMID:30419856.
[25] Liu P, Ge M, Hu J, Li X, Che L, Sun K, *et al*. A functional mammalian target of rapamycin complex 1 signaling is indispensable for c-Myc-driven hepatocarcinogenesis. Hepatology 2017;66(1):167–181. doi:10.1002/hep.29183, PMID:28370287.
[26] Albakova Z. HSP90 multi-functionality in cancer. Front Immunol 2024;15:1436973. doi:10.3389/fimmu.2024.1436973, PMID:39148727.
[27] Baird L, Yamamoto M. The Molecular Mechanisms Regulating the KEAP1-NRF2 Pathway. Mol Cell Biol 2020;40(13):e00099–20. doi:10.1128/MCB.00099-20, PMID:32284348.
[28] Wang Y, Deng B. Hepatocellular carcinoma: molecular mechanism, targeted therapy, and biomarkers. Cancer Metastasis Rev 2023;42(3):629–652. doi:10.1007/s10555-023-10084-4, PMID:36729264.
[29] Rialdi A, Duffy M, Scopton AP, Fonseca F, Zhao JN, Schwarz M, *et al*. WNTinib is a multi-kinase inhibitor with specificity against β-catenin mutant hepatocellular carcinoma. Nat Cancer 2023;4(8):1157–1175. doi:10.1038/s43018-023-00609-9, PMID:37537299.
[30] Toh TB, Lim JJ, Hooi L, Rashid MBMA, Chow EK. Targeting Jak/Stat pathway as a therapeutic strategy against SP/CD44+ tumorigenic cells in Akt/β-catenin-driven hepatocellular carcinoma. J Hepatol 2020;72(1):104–118. doi:10.1016/j.jhep.2019.08.035, PMID:31541681.
[31] Adebayo Michael AO, Ko S, Tao J, Moghe A, Yang H, Xu M, *et al*. Inhibiting Glutamine-Dependent mTORC1 Activation Ameliorates Liver Cancers Driven by β-Catenin Mutations. Cell Metab 2019;29(5):1135–1150.e6. doi:10.1016/j.cmet.2019.01.002, PMID:30713111.
[32] Yi J, Zhu J, Wu J, Thompson CB, Jiang X. Oncogenic activation of PI3K-AKT-mTOR signaling suppresses ferroptosis via SREBP-mediated lipogenesis. Proc Natl Acad Sci U S A 2020;117(49):31189–31197. doi:10.1073/pnas.2017152117, PMID:33229547.
[33] Panwar V, Singh A, Bhatt M, Tonk RK, Azizov S, Raza AS, *et al*. Multifaceted role of mTOR (mammalian target of rapamycin) signaling pathway in human health and disease. Signal Transduct Target Ther 2023;8(1):375. doi:10.1038/s41392-023-01608-z, PMID:37779156.
[34] Luo Z, Zheng Q, Ye S, Li Y, Chen J, Fan C, *et al*. HMGA2 alleviates ferroptosis by promoting GPX4 expression in pancreatic cancer cells. Cell Death Dis 2024;15(3):220. doi:10.1038/s41419-024-06592-y, PMID:38493165.
[35] Wang C, Cigliano A, Jiang L, Li X, Fan B, Pilo MG, *et al*. 4EBP1/eIF4E and p70S6K/RPS6 axes play critical and distinct roles in hepatocarcinogenesis driven by AKT and N-Ras proto-oncogenes in mice. Hepatology 2015;61(1):200–213. doi:10.1002/hep.27396, PMID:25145583.
[36] Liu Y, Qiu S, Huang H, Wu Z, Ge S. Ferrostatin supplementation improves microalgal activities and nutrient removal in wastewater under high temperature shock: From ferroptosis-like inhibition to enhanced oxidation resistance. Water Res 2025;273:123033. doi:10.1016/j.watres.2024.123033, PMID:39721506.
[37] Prince TL, Kijima T, Tatokoro M, Lee S, Tsutsumi S, Yim K, *et al*. Client Proteins and Small Molecule Inhibitors Display Distinct Binding Preferences for Constitutive and Stress-Induced HSP90 Isoforms and Their Conformationally Restricted Mutants. PLoS One 2015;10(10):e0141786. doi:10.1371/journal.pone.0141786, PMID:26517842.
[38] George DJ, Halabi S, Healy P, Jonasch D, Anand M, Rasmussen J, *et al*. Phase 2 clinical trial of TORC1 inhibition with everolimus in men with metastatic castration-resistant prostate cancer. Urol Oncol 2020;38(3):79.e15–79.e22. doi:10.1016/j.urolonc.2019.08.015, PMID:31522863.
[39] Caro-Vegas C, Bailey A, Bigi R, Damania B, Dittmer DP. Targeting mTOR with MLN0128 Overcomes Rapamycin and Chemoresistant Primary Effusion Lymphoma. mBio 2019;10(1):e02871–18. doi:10.1128/mBio.02871-18, PMID:30782662.
[40] Liu H, Yao Y, Zhang J, Li J. MEK inhibition overcomes everolimus resistance in gastric cancer. Cancer Chemother Pharmacol 2020;85(6):1079–1087. doi:10.1007/s00280-020-04078-0, PMID:32444897.
[41] Mohammed Abdul KS, Han K, Guerrero AB, Wilson CN, Kulkarni A, Purcell NH. Increased PHLPP1 expression through ERK-4E-BP1 signaling axis drives nicotine induced oxidative stress related damage of cardiomyocytes. J Mol Cell Cardiol 2024;193:100–112. doi:10.1016/j.yjmcc.2024.05.014, PMID:38851627.
[42] Lioulia E, Mokos P, Panteris E, Dafou D. UBE2T promotes β-catenin nuclear translocation in hepatocellular carcinoma through MAPK/ERK-dependent activation. Mol Oncol 2022;16(8):1694–1713. doi:10.1002/1878-0261.13111, PMID:34614271.
[43] Üremiş MM, Üremiş N, Türköz Y. Cucurbitacin E shows synergistic effect with sorafenib by inducing apoptosis in hepatocellular carcinoma cells and regulates Jak/Stat3, ERK/MAPK, PI3K/Akt/mTOR signaling pathways. Steroids 2023;198:109261. doi:10.1016/j.steroids.2023.109261, PMID:37355001.
[44] Wang P, Song X, Utpatel K, Shang R, Yang YM, Xu M, *et al*. MEK inhibition suppresses K-Ras wild-type cholangiocarcinoma in vitro and in vivo via inhibiting cell proliferation and modulating tumor microenvironment. Cell Death Dis 2019;10(2):120. doi:10.1038/s41419-019-1389-4, PMID:30741922.